

# Electronically Tunable Ferroelectric Devices for Microwave Applications

Stanis Courrèges<sup>1</sup>, Zhiyong Zhao<sup>2</sup>, Kwang Choi<sup>2</sup>,  
Andrew Hunt<sup>2</sup> and John Papapolymerou<sup>1</sup>

<sup>1</sup> *School of Electrical and Computer Engineering, Georgia Institute of Technology*

<sup>2</sup> *nGimat Co.*

*USA*

## 1. Introduction

Tunable microwave devices provide added functionality, smaller form factor, lower cost, and lighter weight, and are in great demand for future communications and radar applications. Available tunable technologies include ferrites, semiconductors, microelectromechanical systems (MEMS), and ferroelectric thin films. While each technology has its own pros and cons, ferroelectric thin film based technology has attracted much attention due to its simple processes, low power consumption, high power handling, small size, and fast tuning. This chapter is not intended to provide an exhaustive overview of the ferroelectric technology, but to present several key points in materials optimization, capacitor structure, and device designs that Georgia Institute of Technology and nGimat have focused on in the last few years. Interested readers are suggested to read the large number of books, book chapters, review papers, workshop notes, and patents that are available (for example, Lancaster et al., 1998; Xi et al., 2000; York & Pond, 2000; Tagantsev et al., 2003; Jakoby et al., 2004).

## 2. Ferroelectric Technology

Ferroelectric material is a category of material with reorientable spontaneous polarization, a sub-category of pyroelectric materials. Because of their high dielectric constant and high breakdown voltage, ferroelectric materials have a wide range of applications: infrared (IR) detectors for security systems and navigation, high density capacitors, high-density DRAMs, non-volatile ferroelectric memory, and high frequency devices such as varactors, frequency multipliers, delay lines, filters, oscillators, resonators and tunable phase shifters (Chang et al., 1998; Cole et al., 2000; Fuflyigin et al., 2000; Joshi & Cole, 2000).

Among these applications, frequency agile devices based on ferroelectric thin films attract much research and development. Barium strontium titanate ( $\text{Ba}_{1-x}\text{Sr}_x\text{TiO}_3$  or BST) is the most studied ferroelectric material for tunable applications. A great characteristic of BST is that STO and BTO can form solid solution with virtually any value of  $x$ , as a result its dielectric properties varies in a relatively predictable fashion. While the Curie temperature of STO is

below 0 K, it is about 120° C for BTO. When  $x$  is varied, the Curie temperature of  $Ba_{1-x}Sr_xTiO_3$  changes accordingly. At temperatures above the Curie temperature, the material is said to be at the paraelectric state, and below the Curie temperature, the material is at the ferroelectric state, in which hysteresis exists. Nearly all-tunable BST devices are operated at the paraelectric state of the BST to reduce dielectric loss and eliminate hysteresis.

Bulk BST materials were studied decades ago, and their dielectric properties are well known. However, the high voltages (e.g., 1000's V) required to bias the bulk BST prevent it from many portable and commercial applications, and thin film BST becomes a good alternative. Even though thin film BST does not show the same dielectric properties as a bulk one, its tunability at low DC bias voltages (e.g., 2:1 tuning has been achieved at a bias of 10 V) opens door for many applications.

It is recognized that the technique used to deposit BST films plays a major role in determining the film's material properties, and consequently its dielectric and electrical properties. Several techniques are available to deposit BST films, such as RF sputtering (Chu & Lin, 1997), pulsed laser ablation deposition (PLD) (Bhattacharya et al., 1994), metal-organic deposition (MOD) (Fijii et al., 1992), chemical vapor deposition (CVD) (Yamamuka et al., 1998), metal-organic chemical vapor deposition (MOCVD) (Gao et al., 2000), and sol-gel processing (Zeng et al., 1999). In order to be successful, the process must be economical and the resultant films must exhibit controlled composition, good thickness uniformity, high density, a high degree of structural perfection, and required electrical properties. High quality BST thin films have been deposited by using MOCVD and PLD. However, these processes are expensive, require costly starting materials, and have low throughput and low yield due to composition variations and defects. The recently developed open atmosphere, low cost combustion chemical vapor deposition (CCVD) technology (Hunt et al., 1993) offers an attractive alternative to grow epitaxial BST thin films on sapphire substrates (Schmitt et al., 2006) with good yield and high throughput potential.

Despite the enormous application potential, the progress in ferroelectric technology has been elusive primarily due to the following reasons: (1) the loss was still high compared to its counterparts, attributed to the poor crystalline quality, (2) a process of making high-quality, large-area BST at reasonable cost did not exist, (3) the required DC bias voltage was too high (~100 V) or intermodulation distortion (IMD) performance was poor, and/or (4) the responses of the BST devices are temperature dependent.

In this chapter, we present some of our research and development results including materials development, capacitor structures, and device designs.

- Epitaxial BST thin films on inexpensive sapphire substrates (Zhao et al., 2006),
- Innovative capacitor structure that requires low DC bias voltage and shows improve IMD performance (Yoon et al., 2003),
- Tunable filters operated at microwave (6-20 GHz) and millimeter wave (30-45 GHz) frequencies (Courrèges et al. 2009; Papapolymerou et al., 2006; Lugo et al., 2007),
- Phase shifters operated at L- to C-band and up to Ka-band (nGimat, 2005; Kenney et al., 2006; Zhao et al., 2007).

### 3. Ferroelectric BST Materials and Varactors

#### 3.1 Epitaxial BST on Sapphire Substrate

In the CCVD process (Fig. 1), precursors, which are the metal-bearing chemicals used to coat an object, are dissolved in a solution, which typically is a combustible fuel. This solution is atomized to form microscopic droplets by means of the proprietary Nanomiser® Device. These droplets are then carried by an oxygen stream to the flame where they are combusted. A substrate (the material being coated) is coated by simply drawing it in front of the flame. The heat from the flame provides the energy required to vaporize the droplets and for the precursors to react and deposit (condense) on the substrates.

The key advantages of the CCVD technology include:

- Open-atmosphere processing,
- Use of inexpensive, environmentally friendly, soluble chemical reagents,
- Production of tailored and complex material.

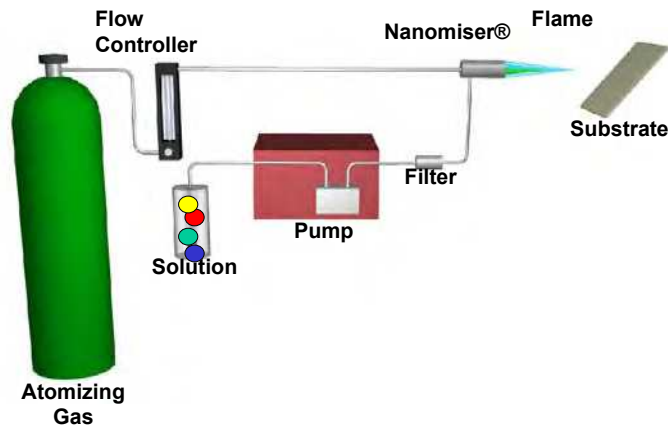


Fig. 1. Schematic representation of the CCVD system.

It is known that epitaxial BST films exhibit greater dielectric constant and tunability as well as lower loss tangent. Historically, complex oxides in the RF/microwave domain, such as BST, have not been applied to commercial products due to the difficulty in producing high-quality thin films. nGimat has developed its proprietary CCVD process for depositing epitaxial BST dielectric coatings on sapphire that provide the building blocks for a host of microwave and RF broadband devices. nGimat's significant advantage is the fact that the CCVD process can deposit BST thin films at lower costs and with better material properties, compared to other manufacturing processes.

Sapphire is chosen as the substrate because of its good insulating properties, low loss tangent, lower cost compared to MgO, LaAlO<sub>3</sub>, and SrTiO<sub>3</sub>, and availability of large size substrates (6" sapphire substrates available). Sapphire has a hexagonal crystal structure with  $a = 4.759 \text{ \AA}$  and  $c = 12.99 \text{ \AA}$ , but Ba<sub>1-x</sub>Sr<sub>x</sub>TiO<sub>3</sub> is cubic when  $x = 1$  (SrTiO<sub>3</sub>), with a lattice parameter of  $3.905 \text{ \AA}$ , and tetragonal when  $x = 0$  (BaTiO<sub>3</sub>), with  $a = 3.994 \text{ \AA}$  and  $c = 4.038 \text{ \AA}$ . We have developed an interface nanolayer between BST and sapphire that enabled an epitaxial BST growth. Fig. 2 shows an SEM micrograph of a cross section of a CCVD BST

thin film as well as a corresponding x-ray diffraction pole figure showing epitaxy between the coating and an r-sapphire substrate.

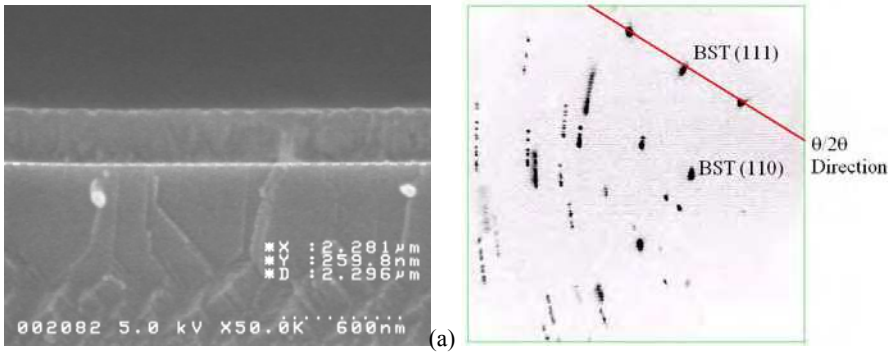


Fig. 2. (a) An SEM microphotograph of the cross section of a BST film. (b) Area detector XRD patterns.

### 3.2 BST Varactors

The core of a BST tunable device is a tunable capacitor, in which BST is the dielectric material. BST capacitors can be fabricated using parallel-plate or planar configurations. Parallel-plate thin film structures require lower tuning DC voltages (e.g., < 10 V), but the fabrications are sophisticated due to the patterning and etching of the bottom electrode and BST. Furthermore, the growth of a highly crystalline and defect-free BST film requires a chemically compatible and durable bottom electrode, which is electrically conductive at microwave frequencies. Pt has been the primary bottom electrode for the parallel-plate BST capacitors, but its poor conductivity leads to high device losses.

In contrast, planar configurations require fewer lithography steps, and single crystal substrates can be used to grow epitaxial BST films. But limited by the photolithographical techniques, the gap width of a planar capacitor is typically in the range of a few microns. This requires larger bias voltage to achieve the desired tunability. Georgia Institute of Technology and nGimat have developed an innovative planar capacitor structure (Yoon et al., 2003) that not only reduces bias voltage for the same tunability but also improves IMD performance.

The improved structure is shown schematically in Fig. 3. Both DC bias and RF signal are applied on the high conductive metal electrodes. The high resistivity electrode (e.g., indium tin oxide) fingers provide a constant DC bias voltage to the BST film, but they are “invisible” to RF signal due to their high impedance. Two-tone IMD tests at 1.9 GHz show that the IMD performance for the novel structure is improved by 6 dBm over the conventional reference structure ( $IIP_3 = 52$  dBm). Another beneficial outcome of this structure is that it allows for lower DC bias required to obtain the same tuning. Fig. 4 shows the tunability curve of the new capacitor structure. Q factor at 1 MHz is not reported due to the fact that it is not a good indicator of the loss tangent at microwave frequencies. Often times, it is misleading to report a higher Q at *megahertz*, while the devices are designed for *gigahertz* applications.

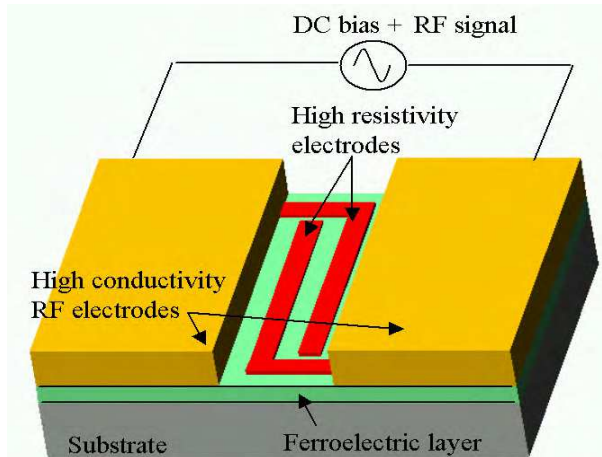


Fig. 3. An innovative planar capacitor structure that requires lower DC bias voltages and exhibits improved IMD performance.

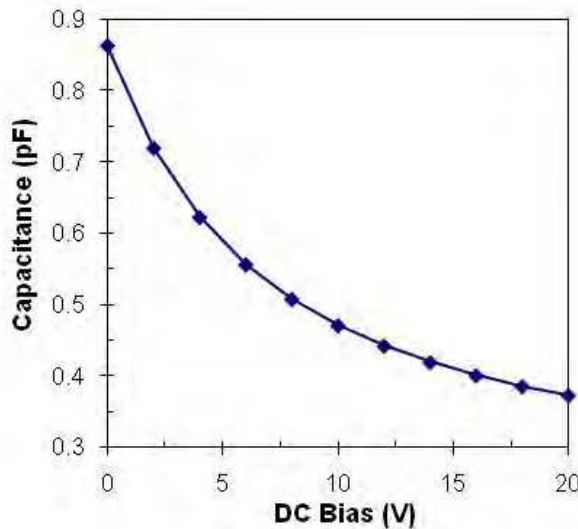


Fig. 4. Capacitance at 1 MHz versus tunability for the new planar capacitor.

## 4. Microwave and Millimetre-Wave Tunable Ferroelectric Filters

### 4.1 Interest of electronically tunable ferroelectric filters

With the pervasive growth of electronic systems in the defense and commercial marketplaces, there is a need for the development of microwave filters with compact size, inexpensive manufacturing process and precise filter response synthesis. Tunable filters are

a good alternative to switchable filter banks by offering smaller size and lower power consumption and requiring a simpler and lower-cost process. Tunable filters for wireless front-end applications have already been demonstrated using RF-MEMS switches (Palego et al, 2008; Park & Rebeiz, 2008), ferroelectric capacitors (Pleskachev & Vendik, 2004; Papapolymerou et al, 2006; Feng et al, 2009), and PIN diodes (Rauscher, 2003). The performance of these reconfigurable circuits mainly relies on these tunable components, and frequency reconfigurable filters are particularly sensitive to loss. Low-loss tunable filters based on PIN diodes are limited to frequencies below 5 GHz since the series resistance of the diodes increases considerably as frequency increases, resulting in high insertion loss. Even though better insertion loss can be achieved at high frequencies for RF-MEMS technology, the filters using these conventional components can only be switched in the microsecond range. The switches also need hermetic packaging. Furthermore, agile filters using PIN diodes or RF-MEMS are usually switchable filters and do not allow an analog frequency tuning. Unlike PIN diodes and RF-MEMS switches, ferroelectrics BST thin films represent an interesting way to design reconfigurable filters since their permittivity can be tuned in an analog way and the switching time is in the nanosecond range.

As explained above, nGimat's epitaxial BST on sapphire technology enables the fabrication of low-loss planar capacitors, simplifying the fabrication process and resulting in lower metal losses. The innovative tunable capacitor structure reduces the DC bias and improves the intermodulation distortion performance. This technology has been employed to design several electronically tunable ferroelectric filters with good performances for X-band and Ka-band applications.

#### 4.2 Method of simulation

Suitable electromagnetic software has to be used to design tunable devices, which includes ferroelectric thin-films. Indeed, for many reasons, these circuits are difficult to be rigorously simulated. First of all, there is an important difference between the thickness of ferroelectric layers (hundreds of nanometers) and the thickness of substrates (hundreds of micrometers), where the ferroelectric is deposited. For example, 2D simulation software, which includes the real topology, the layers of tunable elements and other metallization parts of the circuit, are not adequately efficient because the meshing elements of thin-films provide big approximations in the calculation. 3D electromagnetic softwares solve Maxwell's equations with the finite element method and must absolutely simulate with a high density of meshing, which increases the calculation time and the needed memory significantly. Secondly, the tuning of ferroelectric devices comes from the variation of ferroelectric material permittivity, which is not uniform in the 3D structure. For example, (Courrèges et al, 2007) presented these non-uniform effects in ferroelectric layers for tunable microstrip and coplanar resonators. Fast calculations were computed with 2D/3D analysis software developed at XLIM research institute (France), which takes into account the effects of inhomogeneous layers (ferroelectric thin-film and substrate) using a small computer memory. However, the time needed to draw complex topologies can be long.

The designs developed by Georgia Institute of Technology and nGimat use lumped-element model for BST tunable capacitors, while other metallization layers are simulated using their 3D structures. For our studies, we use commercial electromagnetic simulation software such as Agilent's ADS-Momentum (2½D), SONNET (2½D), or Ansoft's HFSS (3D). Hybrid

simulation approach consists in combining the electromagnetic calculation of the topology with the lumped element model of BST tunable capacitors, included in the filter design. Fig. 5 presents a simulation example of a Ka-band tunable ferroelectric filter with the software ADS. Identical simulations can be run using other softwares, such as those listed above.

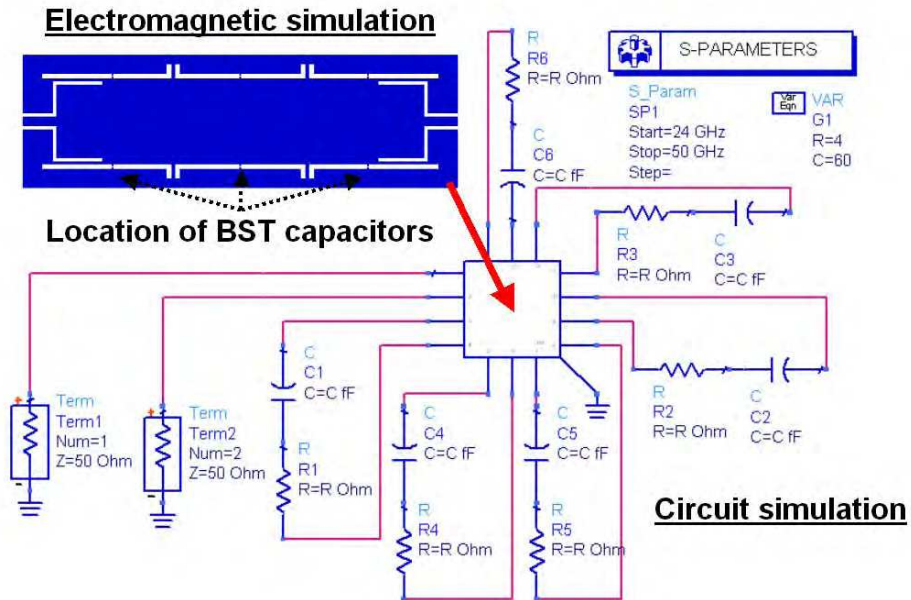


Fig. 5. Simulation of a Ka-band filter combining the electromagnetic calculation with the capacitive-resistive effects of BST capacitors.

Electromagnetic calculation of the filter (real pattern in blue color, in Fig. 5) is coupled with a schematic simulation. Two highly resistive internal ports are placed at the capacitor location. The method takes into account the capacitive-resistive effect of each BST varactor by connecting a lumped-element capacitor  $C$  with a series resistor  $R$  between both internal ports. The capacitor  $C$  ranges from the minimal and maximal capacitance value when the BST capacitors are biased by external DC voltages. The resistor  $R$  represents the overall loss of the ferroelectric capacitors. The values  $C$  and  $R$  are determined after an RF-characterization of the single BST capacitors. When BST tunable capacitor chips are connected to circuits with bonding-wires, the simulation has to take into account an additional series inductive effect. The value of the inductance mostly depends on the length and the diameter of wires at the working frequency.

### 4.3 X-band tunable ferroelectric filters

Compact 4-pole quasi-elliptic planar filters including epitaxial ferroelectric BST capacitors were designed on sapphire for X-band active electronically steered antenna (AESAs) arrays used in radar systems (Fig. 6) (Courrèges et al, 2009). This is the first time that a complex topology has been fabricated with the ferroelectric technology to meet the stringent

specifications: number of resonators, selectivity, flat bandwidth, high unloaded quality factor and compactness.

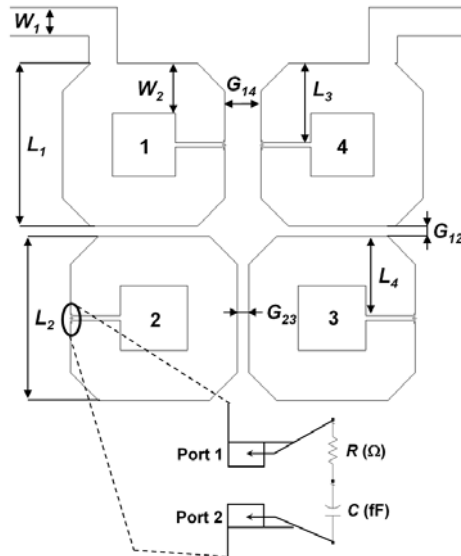


Fig. 6. Design of the 4-pole quasi-elliptic tunable filter including ferroelectric BST capacitors.

The frequency tuning required for the application is below 10%. The other specifications for the first filter are: a fractional 1-dB bandwidth between 5% and 8%, an insertion loss of over 30 dB at  $\pm 10\%$  of the central frequency ( $f_0$ ), a frequency tuning of about 650 MHz, an insertion loss in the bandwidth as low as possible and a maximum footprint of 10 mm x 10 mm.

The fabricated filter is composed of 4 cross-coupled open-loop resonators to meet the specifications. The four half-wavelength resonators are loaded by the BST tunable capacitors between both ends (1 BST capacitor for each resonator), which allow tuning of the center frequency by applying DC voltages. Since the electric field is maximum at the end of the resonator (capacitive part), a maximum frequency shift can be provided by loading with an external capacitor, which also reduces the initial length of the resonators  $\lambda_g/2$ , where  $\lambda_g$  is the guided wavelength with the fundamental resonant frequency ( $f_0$ ). The width of the resonators is increased to get smaller resonator impedances of 37  $\Omega$  and consequently a higher unloaded quality factor  $Q_0$ . The 50- $\Omega$  input and output feedlines are physically connected to resonators 1 and 4, respectively, to get the proper input-output impedances. The filter is made on a sapphire substrate with a thickness of 430  $\mu\text{m}$ . Its relative permittivity is  $\epsilon_r \text{Sapphire} = 10$  and its loss tangent is below  $10^{-4}$ . The copper metallization of the resonators and the ground plane is 2- $\mu\text{m}$  thick with a conductivity of  $5.10^7 \text{ S/m}$ .

As described in section 4.2, a hybrid simulation approach coupled to the electromagnetic segmentation method (Bariant et al, 2002) is employed to optimize the S-parameter responses of the filter. We choose the normalized coupling matrix  $M_1$  for the required filter



specifications (Eq. 1).

$$[M_1] = \begin{bmatrix} 0 & 1.012 & 0 & -0.12 \\ 1.012 & 0 & 0.812 & 0 \\ 0 & 0.812 & 0 & 1.012 \\ -0.12 & 0 & 1.012 & 0 \end{bmatrix} \quad (1)$$

$$R_{in} = R_{out} = 1.143$$

The input/output impedances ( $R_{in}$  and  $R_{out}$ ) and the mutual inter-resonator coupling  $M_{ij}$  are used to find the external quality factor  $Q_{ext}$ , and the inter-resonator coupling  $k_{ij}$ . Then, the simulated S-parameters of the filter are optimized by adjusting  $Q_{ext}$ , and  $k_{ij}$  versus the filter dimensions: lengths of the resonators, positions of the feedlines and the gaps between the resonators. A final optimization of dimensions allows getting the right frequency responses (Table 1). The final size is very compact at this frequency: 5.7 mm x 5.5 mm. A photograph of the fabricated filter is shown in Fig. 7.

Parameter	( $\mu\text{m}$ )	Parameter	( $\mu\text{m}$ )	Parameter	( $\mu\text{m}$ )
$W_1$	407	$L_2$	1140	$G_{14}$	520
$W_2$	715	$L_3$	2360	$G_{12}$	145
$L_1$	2341	$L_4$	1144	$G_{23}$	168

Table 1. Optimized dimensions for the first filter design.

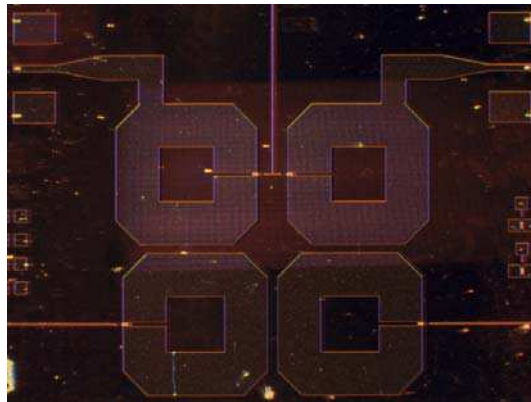


Fig. 7. Photograph of the first fabricated filter.

The DC bias is applied through bias tees. High-resistive thin strips are connected between the resonators in order to bias the resonators 2 and 3. The bias lines for the ground are connected to a copper square ring around the filter to use only one DC probe for the common ground. Coplanar pads are added to create vialess CPW transitions (Zheng et al, 2003) at the end of the feedlines to enable measurement using G-S-G probes. The measurements are performed with an Agilent Vector Network Analyzer 8510C calibrated

using the Short-Open-Load-Through (SOLT) standards and a pair of 800- $\mu\text{m}$  pitch probes (GGB Picoprobe). The S-parameters are measured with bias voltages ranging from 0 V to 30 V (Figs. 8 and 9).

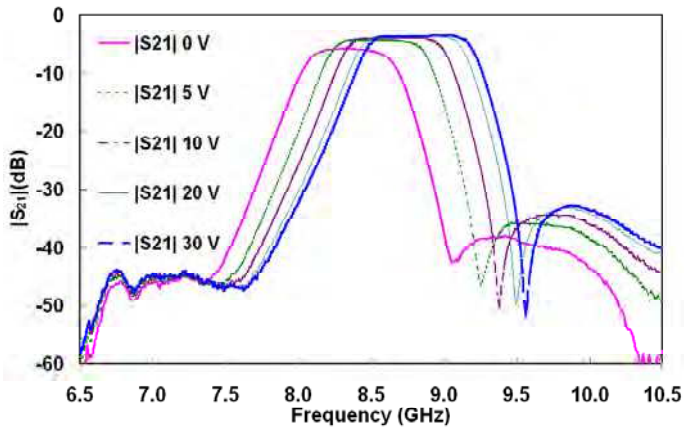


Fig. 8. Measured  $|S_{21}|$  of the 4-pole quasi-elliptic tunable filter.

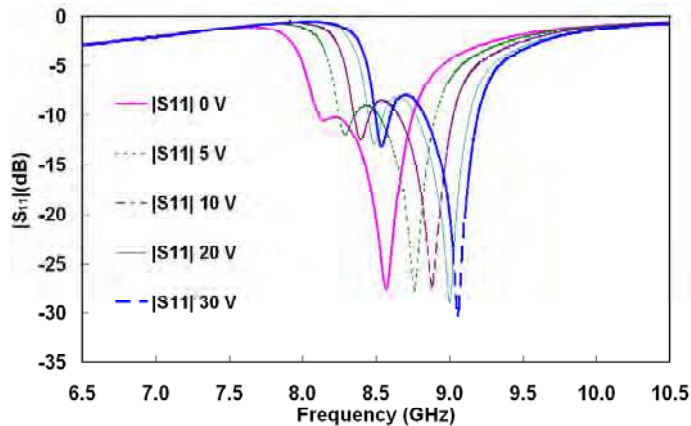


Fig. 9. Measured  $|S_{11}|$  of the 4-pole quasi-elliptic tunable filter.

The center frequency at 0 V is 8.35 GHz and the filter reaches a maximum frequency tuning of 500 MHz (6%) with a bias voltage of 30 V. The fractional 1-dB bandwidth ranges from 5.5% to 7.3%. The filter has an insertion loss and a return loss in the bandwidth of 5.7-3.5 dB, and 10.2-7.9 dB, respectively, between a DC bias of 0 V and 30 V. The insertion loss outside the passband is 30 dB as desired. By taking into account the values of the bandwidth, the frequency and the return loss, the unloaded quality factor is between 80 (0 V) and 115 (30 V). The measured results present very good loss performances for typical X-band tunable ferroelectric filters at room temperature.

This filter, with other values of bandwidth and center frequency, was improved with a second similar design (Fig. 10).

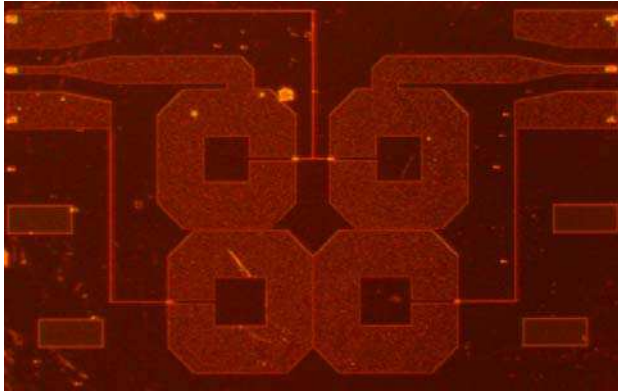


Fig. 10. Photograph of the second fabricated filter.

The biasing of the capacitors is realized with bias tees by applying DC bias on RF signal (positive DC bias) and RF ground (DC ground). To bias resonators 2 and 3, which do not have direct connection with the feedlines, the design uses high-resistive thin strips connected between the resonators 1 and 2, 2 and 3, and 3 and 4. The filter has a size of 4.9 mm x 4.9 mm. The experimental results are presented in Figs 11. and 12.

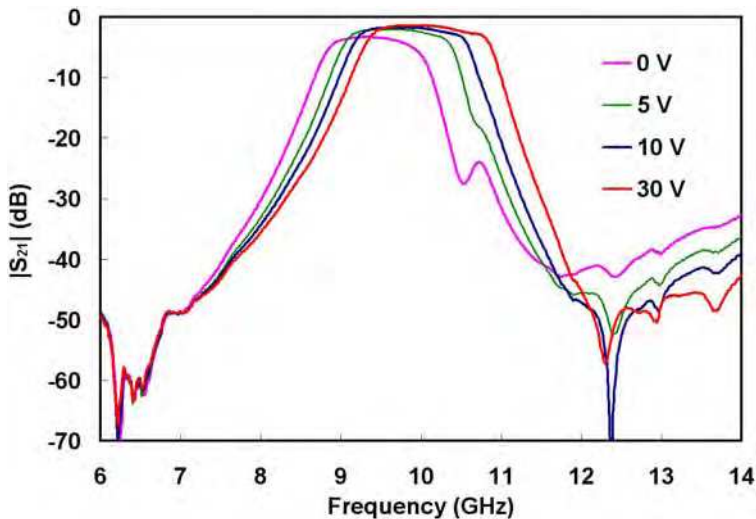


Fig. 11. Measured  $|S_{21}|$  of the second 4-pole tunable filter.

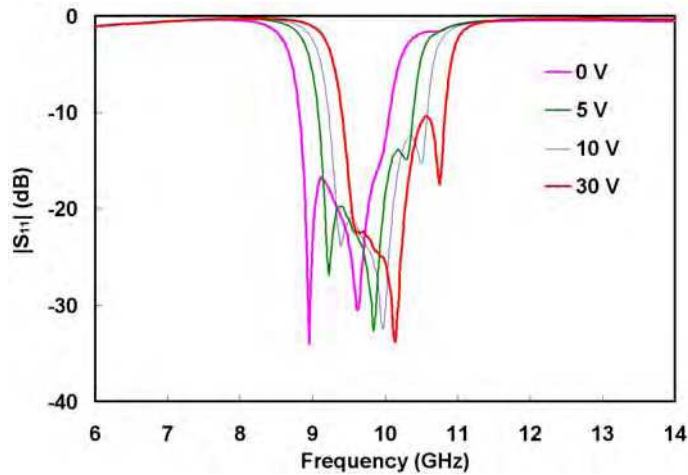


Fig. 12. Measured  $|S_{11}|$  of the second 4-pole tunable filter.

The center frequency of the second filter is 9.37 GHz without bias voltage. The frequency tuning at 30 V is 690 MHz (7.4%) that is better than the previous result. The fractional 1-dB bandwidth ranges from 11.4% up to 13.8%. The insertion loss and return loss in the passband are excellent, and better than those presented for the first design: 3.3-1.4 dB and 17-11 dB, respectively, between a DC bias of 0 and 30 V. This filter presents a low level of insertion loss and a good selectivity with the ferroelectric technology. The unloaded quality factor of the filter with a DC bias of 30 V is better than 130, an improvement with this second design.

For the same resonator topology, when we also added more BST tunable capacitors, which could be biased independently, allowing controlling the following three parameters independently and continuously: center frequency, bandwidth and return loss in the passband. Experimental results are presented in Figs. 13 and 14.

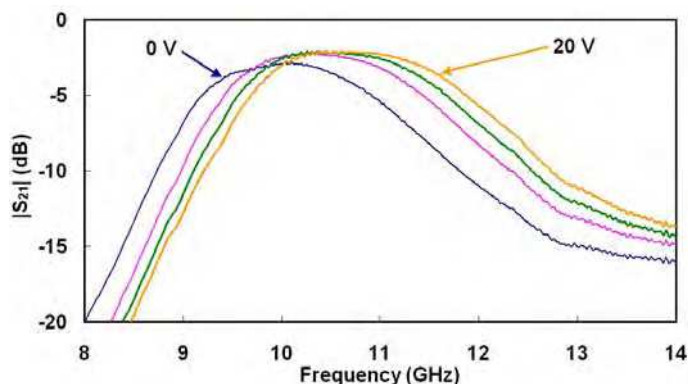


Fig. 13. Measured  $|S_{21}|$  of a 2-pole ferroelectric filter with constant fractional bandwidth.

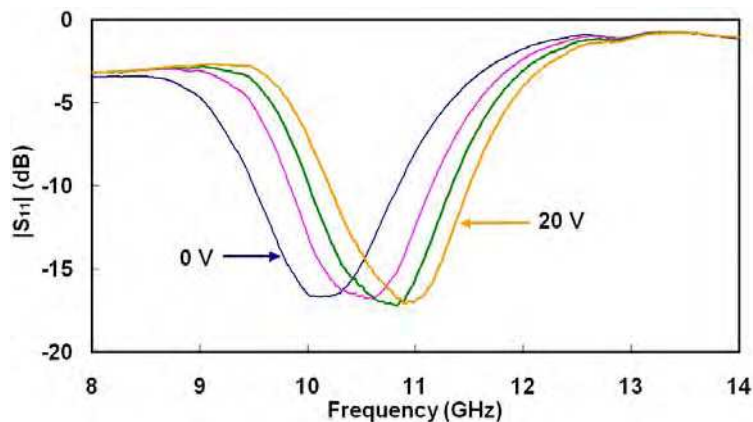


Fig. 14. Measured  $|S_{11}|$  of a 2-pole ferroelectric filter with constant fractional bandwidth.

The center frequency without bias voltage is 10 GHz and the frequency tuning is 740 MHz with a DC bias (controlling the resonant frequency) of 20 V (7.4%). The fractional equal-ripple bandwidth and the return loss are almost constant for all states of frequency: 8.1% ( $\pm 0.04\%$ ) and 16.7 dB ( $\pm 0.3\%$ ), respectively. Also, the insertion loss in the passband is great, between 2.75 dB and 2.2 dB.

These results open an interesting perspective for the design of complex tunable filtering functions. The third order intercept point (IP3) of these filters was measured by using a two-tone method. The output IP3 values are better than 20 dBm. The results are summarized in Table 2.

	Type	Band	Bandwidth	Insertion Loss: dB	$Q_0$	Tuning	Bias	Size (mm)
1 <sup>st</sup> design	4 poles microstrip Quasi-elliptic	X	5.5-7.3%	5.7-3.5	80-115	6%	30 V	5.7x5.5 Sapphire
2 <sup>nd</sup> design	4 poles microstrip Quasi-elliptic	X	11.4-13.8%	3.3-1.4	<130	7.4%	30 V	4.9x4.9 Sapphire
/	2 poles microstrip	X	8.5%	2.7-2.0	<100	Frequency Bandwidth Return loss 8.3% (max)	30 V	7x3 Sapphire

Table 2. Comparison between the designed X-band tunable ferroelectric filters.

#### 4.4 Ka-band tunable ferroelectric filters

Ferroelectric Ka-band tunable filters, working at room temperature, have been designed for commercial and defense applications. We present one coplanar design developed at 29 GHz (Courrèges et al, 2009). The filter is a 3-pole tunable bandpass filter working in the Ka-band (26-40 GHz), a fractional bandwidth of 10-12 %, a return loss of 20 dB, a frequency tuning greater than 15% and a minimum OIP3 value of 15 dBm. Fig. 15 presents the coplanar filter loaded with 6 BST capacitors (3 on each side).

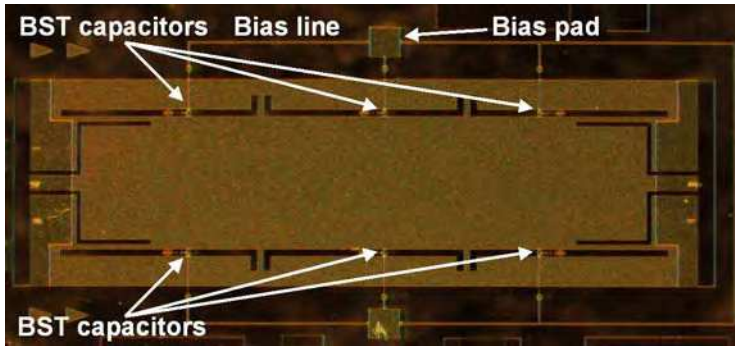


Fig. 15. Photograph of the fabricated Ka-band coplanar ferroelectric filter.

The filter is designed with 3 half-wavelength resonators and inductive impedance inverters. Since the electric field is maximal at the center of each resonator, the maximum frequency shift is achieved by loading the tunable capacitors at this position. The filter is fed by original feedlines (Paillot et al, 2002): the first part is a 50- $\Omega$  line connected to a wider short-circuited line. The filter does not need bridges with this feeding structure and the external quality factor can be easily optimized. It is also possible to get a wider resonator by keeping the same slot gap, which can increase the unloaded quality factor of the filter. The simulation procedure, the materials and the fabrication process are the same as those indicated in the section 4.3 with the X-band tunable filters. The final filter size is 4560 x 1400  $\mu\text{m}$ . The experimental S-parameters are presented in Figs. 16 and 17.

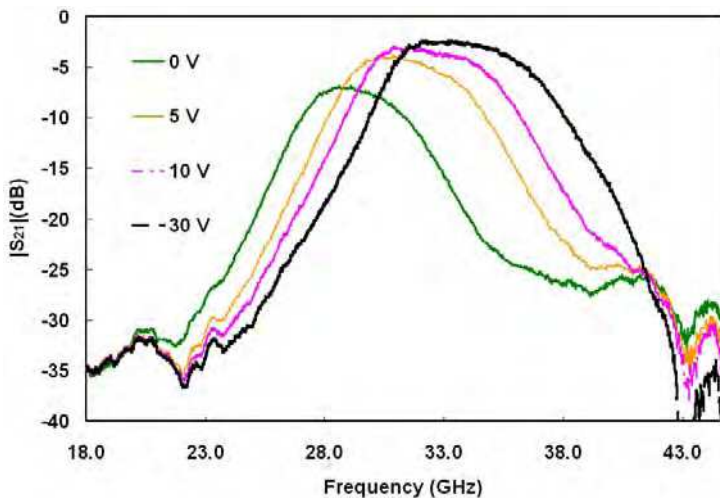


Fig. 6. Measured  $|S_{21}|$  of the Ka-band ferroelectric filter.

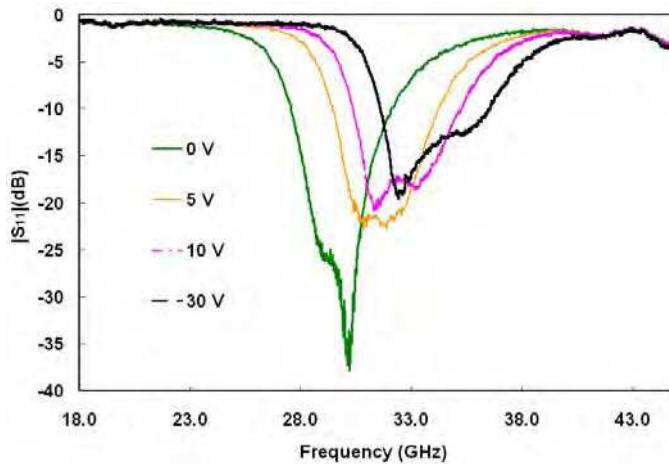


Fig. 17. Measured  $|S_{11}|$  of the Ka-band ferroelectric filter.

The S-parameters are measured with bias voltages ranging from 0 V up to 30 V. The frequency tunes from 29 GHz, at 0 V, up to 34 GHz with a bias voltage of 30 V. The frequency tuning is 17.2%. The fractional bandwidth ranges from 9.5% to 12.3%. For this technology in Ka-band, the planar filter has good insertion loss and return loss levels of 6.9-2.5 dB, and 24-13 dB, respectively, between a DC bias of 0 and 30 V at room temperature.

## 5. Ferroelectric phase shifters

Phase shifters are an essential component in electronically scanned phased-array antennas for communications and radar applications, and typically represent a significant amount of the cost, size and weight of producing military tactical antenna array. Jamming and interferers of mobile communication devices can be eliminated via phase shifters while still receiving the desired signal even with the interferer being at the same frequency. Phase shifting technology of choice includes ferrite, MMIC, MEMS, ferroelectrics, and others. Ferrite phase shifter has been very successfully employed in military systems despite its high cost, weight, large size and complex current switching circuitry. GaAs MMIC phase shifters have demonstrated good phase and amplitude error control. However, they involve a relatively large loss and have low power handling capability. MEMS use advanced IC processing techniques, which offer potential integration with GaAs MMIC or CMOS technologies. They provide low insertion loss, high isolation, negligible power consumption, and low IMD. Nevertheless, they require high driving voltage (e.g., 40 V or higher), have low switching speed ( $> 10 \mu\text{s}$ ), and suffer from reliability and packaging issues.

Several design options for BST phase shifters have been proposed (Kozyrev et al., 1998; Kim et al., 2002; Sherman et al., 2001; Kim et al., 2003; De Flaviis et al., 1997; Van Keuls et al., 1999). Reflection-type phase shifters consist of a 3-dB coupler and reflective loads (Kozyrev et al., 1998; Kim et al., 2002; Sherman et al., 2001). While wide bandwidths may be achieved with the reflection type topology, the coupler contributes directly to the insertion loss of the phase shifter, and requires a large portion of the die area. Loaded-line phase shifters are controlled by varying the capacitive loading on a coplanar waveguide transmission line (Lin

et al., 2000). The phase shifters using this topology show large size, and large numbers of capacitors are required for large phase shift, contributing substantial dielectric losses. nGimat and Georgia Tech have designed an S-band phase shifter using an all-pass network topology (Kim et al., 2003), which exhibited small size and low loss.

Fig. 18 shows the equivalent circuit of an all-pass phase shifter using tunable BST capacitors. While the circuit is all lumped elements, the  $L$ - $C$  sections may be considered equivalent to a transmission line of characteristic impedance  $Z_o = \sqrt{L_o / C_o}$ . Multiple phase shifters can be cascaded to achieve higher phase shift. We have achieved best-in-class performance for L-, S-, and C-band phase shifters with the Figure of Merit, defined as phase shift divided by insertion loss, being measured at 75°/dB (Kenney et al., 2006). Using the same topology, we have developed phase shifters up to 40 GHz.

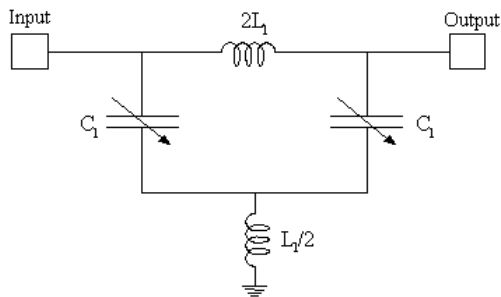


Fig. 18. Schematic of a low-voltage all pass network phase shifter.

Figs. 19 and 20 show, respectively, the measured S-parameters and phase shift of a Ka-band phase shifter. The insertion loss at 0 V is 7 dB, going down to 6 dB quickly at 5 V and even lower at most of the operational range. The return loss is better than 10 dB at all bias states. The phase shift is 370° at 30 V.

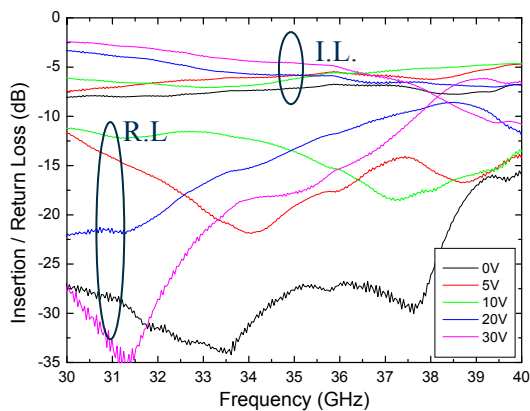


Fig. 19. Measured S-parameters of a 35-GHz phase shifter.



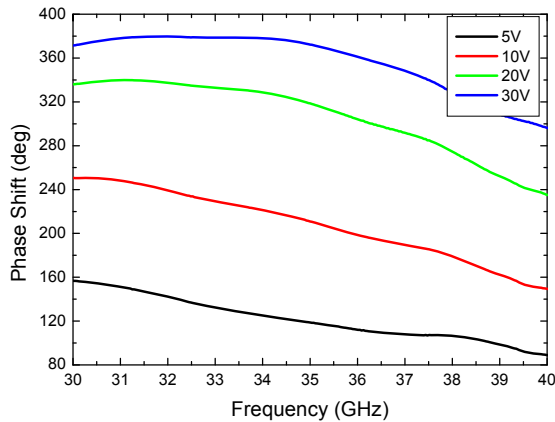


Fig. 20. Measured phase shift of a 35-GHz phase shifter.

Our phase shifters have the following features:

- Small size  $< 1 \times 1$  mm,
- Solder ball terminations for flip-chip mounting,
- Coplanar waveguide input and output to facilitate transitions to the antenna circuitry,
- Lumped-element designs for lower loss,
- Continuously tunable with a single DC bias voltage of 0-30 V,
- Fully passivated to prevent failures due to contaminations,
- No static state power consumption.

## 6. Conclusions

This chapter presents the latest research and development results by Georgia Institute of Technology and nGimat, including materials development, innovative capacitor structure, and device designs. Using proprietary process and interface layers, we are able to grow epitaxial BST films on inexpensive sapphire substrates. A new capacitor structure utilizing highly resistive film improves IMD performance and enables low DC bias voltages. We have used a hybrid design scheme to simulate the circuit, which saves simulation time and memory used. A few design examples are presented including tunable filters and phase shifters covering frequency range up to Ka-band. The devices are easy to fabricate, and exhibit low loss, small size, and low-power consumption.

## 7. References

Bariant, D.; Bila, S., Baillargeat, D., Verdeyme, S. & Guillon, P. (2002). Fast and accurate C.A.D. of narrow band waveguide filters applying an electromagnetic segmentation method, *IEEE Int. Micro. Symp. Dig.*, Vol. 2, (2002) pp. 979-982.

- Bhattacharya, P.; Park, K.H. & Mishioka, Y. (1994). Control of grain structure of laser-deposited  $(\text{Ba,Sr})\text{TiO}_3$  films to reduce leakage current. *Jpn. J. Appl. Phys. Part I*, Vol. 33, No. 9B, (September 1994) pp. 5231-5234.
- Chang, H.; Gao, C., Takeuchi, I., Yoo, Y., Wang, J., Schultz, P.G. & Xiang, X.D. (1998). Combinatorial synthesis and high throughput evaluation of ferroelectric/dielectric thin-film libraries for microwave applications. *Appl. Phys. Lett.*, Vol. 72, No. 17, (1998) pp. 2185-2187.
- Chu, C.M. & Lin, P. (1997). Electrical properties and crystal structure of  $(\text{Ba,Sr})\text{TiO}_3$  films prepared at low temperatures on a  $\text{LaNiO}_3$  electrode by radio-frequency magnetron sputtering. *Appl. Phys. Lett.*, Vol. 70, No. 2, (1997) pp. 249-251.
- Cole, M.W.; Joshi, P.C., Ervin, M.H., Wood, M.C., & Pfeffer, R.L. (2000). The influence of Mg doping on the materials properties of  $\text{Ba}_{1-x}\text{Sr}_x\text{TiO}_3$  thin films for tunable device applications. *Thin Solid Films*, Vol. 374, (2000) pp. 34-41.
- Courrèges, S.; Giraud, S., Cros, D., Madrangeas, V. & Aubourg, M. (2007). 2D and 3D analysis of ferroelectric thin-film planar microwave devices using method of line, *Ferroelectrics*, Vol. 353, (August 2007) pp 124-131.
- Courrèges, S.; Li, Y., Zhao, Z., Choi, K., Hunt, A. & Papapolymerou, J. (2009). A low-loss X-band ferroelectric tunable filter. *IEEE Microwave and Wireless Components Lett.*, Vol. 19, No. 4, (April 2009) pp 203-205.
- Courrèges, S., Li, Y., Zhao, Z., Choi, K., Hunt, A., Horst, S., Cressler, J. D. & Papapolymerou, J. (2009). A Ka-band electronically tunable ferroelectric filter. *IEEE Microwave and Wireless Components Lett.*, Vol. 19, No. 6, (June 2009) pp. 356-358.
- De Flaviis, F.; Alexopoulos, N.G. & Stafsudd, O.M. (1997). Planar microwave integrated phase-shifter design with high purity ferroelectric material. *IEEE Trans. Microwave Theory Tech.*, Vol. 45, No. 6, (June 1997) pp. 963-969.
- Feng, Z.; Fathelbab, W. M., Lam, P. G., Haridasan, V., Maria, J.-P., Kingon, A. I. & Steer, M. B. (2009). Narrowband Barium Strontium Titanate (BST) tunable bandpass filters at X-band. *IEEE Int. Micro. Symp. Dig.*, (June 2009) pp. 1061-1064.
- Fijii, E.; Uemoto, Y., Hayashi, S., Nasu, T., Shimada, Y., Matsuda, A., Kibe, M., Azuma, M., Otsuki, T., Kano, G., Scott, M., McMillan, L.C. & Paz de Araujo, C.A. (1992). ULSI DRAM technology with  $\text{Ba}_{0.7}\text{Sr}_{0.3}\text{TiO}_3$  film of 1.3nm equivalent  $\text{SiO}_2$  thickness and  $10^{-9}$  A/cm<sup>2</sup> leakage current. *IEDM Technical Digest*, (1992) pp. 267-270.
- Fuflyigin, V.; Wang, F., Jiang, H., Zhao J. & Norris, P. (2000). Electro-optic effect in  $\text{Ba}_{1-x}\text{Pb}_x\text{TiO}_3$  films. *Appl. Phys. Lett.*, Vol. 76, No. 13, (2000) pp. 1641-1643.
- Gao, Y.; He, S., Alluri, P., Engelhard, M., Lea, A.S., FINDER, J., Melnick, B. & Hance, R.L. (2000). Effects of precursors and substrate materials on microstructure, dielectric properties, and step coverage of  $(\text{Ba,Sr})\text{TiO}_3$  thin films grown by metalorganic chemical vapor deposition. *J. Appl. Phys.*, Vol. 87, No. 1, (2000) pp. 124-130.
- Hunt, A.T.; Carter, W.B. & Cochran, Jr., J.K. (1993). Combustion chemical vapor deposition: a novel thin-film deposition technique. *Appl. Phys. Lett.*, Vol. 63, No. 2, (July 1993) pp. 266-268.
- Jakoby, R.; Scheele, P., Muller, S. & Weil, C. (2004). Nonlinear dielectrics for tunable microwave components, *Proceedings of 15<sup>th</sup> International Conference on Microwaves, Radar and Wireless Communications (MIKON-2004)*, pp. 369- 378, Warsaw, Poland, May 17-19, 2004.

- Joshi P.C. & Cole, M.W. (2000). Mg-doped Ba<sub>0.6</sub>Sr<sub>0.4</sub>TiO<sub>3</sub> thin films for tunable microwave applications. *Appl. Phys. Lett.*, Vol. 77, No. 2, (2000) pp. 289-291.
- Kenney, J. S.; Yoon, Y. K., Ahn, M., Allen, M. G., Zhao, Z., Wang, X., Hunt, A. & Kim, D. (2006). Low-voltage ferroelectric phase shifters from L- To C-band and their applications, *Proceedings of the 2006 IEEE Aerospace Conference*, 9 ps, Big Sky, MT, March 4-11, 2006, IEEE, Piscataway, NJ.
- Kim, D.S.; Choi, Y.S., Allen, M.G., Kenney, J. S. & Kiesling, D. (2002). A Wide bandwidth monolithic BST reflection-type phase shifter using a coplanar waveguide Lange coupler. *IEEE Trans. Microw. Theory Tech.*, Vol. 50, No. 12, (December 2002) pp. 2903-9.
- Kim, D.S.; Choi, Y. S., Ahn, M., Allen, M.G., Kenney, J.S. & Marry, P. (2003). 2.4 GHz continuously variable ferroelectric phase shifters using all-pass networks. *IEEE Microw. Wireless Comp. Lett.*, Vol. 13, No. 10, (October 2003) pp. 434-36.
- Kozyrev, A.; Ivanov, A., Keis, V., Khazov, M., Osadchy, V., Samoilova, T., Soldatenkov, O., Pavlov, A., Koepf, G., Mueller, C., Galt, D. & Rivkin, T., Ferroelectric films: Nonlinear properties and applications in microwave devices. *IEEE MTT-S 1998 Int. Mi-crowave Symp. Dig.*, (June 1998) pp. 985-988.
- Lancaster, M.J.; Powell, J., & Porch, A. (1998). Thin-film ferroelectric microwave devices. *Supercond. Sci. Technol.*, Vol. 11, (1998) pp. 1323-1334.
- Lugo, C.; Wang, G., Papapolymerou, J., Zhao, Z., Wang, X. & Hunt, A. T. (2007). Frequency and bandwidth agile-mm-wave filter using ferroelectric capacitors and MEMS cantilevers. *IEEE Trans. Microw. Theory Tech.*, Vol. 55, No. 2, (2007) pp. 376-382.
- Paillet, T.; Blondy, P., Cros, D. & Guillon, P.-Y. (2002). A novel compact coplanar filter. *IEEE MTT-S Int. Micro. Symp. Dig.*, Vol. 3, (June 2002) pp. 1793-1796.
- Palego, C.; Pothier, A., Crunteanu, A., Chatras, M., Blondy, P., Champeaux, C., Tristant, P. & Catherinot, A. (2008). A two-pole lumped-element programmable filter with MEMS pseudodigital capacitor banks. *IEEE Trans. on Micro. Theory Tech.*, Vol. 56, No. 3 (March 2008) pp. 729-735.
- Papapolymerou, J.; Lugo, C., Zhao, Z., Wang, X. & Hunt, A. (2006). A miniature low-loss slow-wave tunable ferroelectric bandpass filter from 11-14 GHz, *Proceedings of the IEEE MTT-S International Microwave Symposium*, pp. 556-559, San Francisco, CA, June 11-16, 2006, IEEE, Piscataway, NJ.
- Park, S.-J. & Rebeiz, G.M. (2008). Low-loss two-pole tunable filters with three different predefined bandwidth characteristics, *IEEE Trans. on Micro. Theory Tech.*, Vol. 56, No. 5, (May 2008) pp. 1137-1148.
- Pleskachev, V. & Vendik, I. (2004). Tunable microwave filters based on ferroelectric capacitors. *Microwaves, Radar and Wireless Communications, MIKON-2004*, Vol. 3, May 2004, pp. 1039-1043.
- Rauscher, C. (2003). Reconfigurable bandpass filter with a three-to-one switchable passband width, *IEEE Trans. on Microwave Theory Tech.*, Vol. 51, No. 2, (February 2003) pp. 573-577.
- Schmitt, J.; Cui, G.G., Luten, III, H.A., Yang, F., Gladden, F.A., Flanagan, S., Jian Y. & Hunt A.T. (2006). Electronic and optical materials, U.S. Patent 6,986,955, January 17, 2006.

- Sherman, V.; Astafiev, K., Setter, N., Tagantsev, A., Vendik, O., Vendik, I., Hoffmann, S., Böttger, U. & Waser, R. (2001). Digital reflection-type phase shifter based on a ferroelectric planar capacitor. *IEEE Microw. Wireless Comp. Lett.*, Vol. 11, No. 10, (October 2001) pp. 407-409.
- Tagantsev, A.K.; Sherman, V.O., Astafiev, K.F., Venkatesh, J. & Setter, N. (2003). Ferroelectric materials for microwave tunable applications. *J. Electroceramics*, Vol. 11, (2003) pp. 5-66.
- Van Keuls, F.W.; Mueller, C.H., Miranda, F.A., Romanofsky, R.R., Canedy, C.L., Aggarwal, S., Venkatesan, T., Ramesh, R., Horwitz, J.S., Chang, W. & Kim, W.J. (1999). Room temperature thin film  $\text{Ba}_x\text{Sr}_{1-x}\text{TiO}_3$  Ku-band coupled microstrip phase shifters: effects of film thickness, doping, annealing and substrate choice. *1999 IEEE MTT-S Int. Microwave Symp. Dig.*, pp. 737-740.
- Xi, X.X.; Li, H.-C., Si, W., Sirenko, A.A., Akimov, I.A., Fox, J.R., Clark, A.M., & Hao, J. (2000). Oxide thin films for tunable microwave devices. *J. Electroceramics*, Vol. 4, No. 2/3, (2000) pp. 393-405.
- Yamamuka, M.; Kawahara, T., Yuuki A. & Ono, K. (1998). Reaction mechanism and electrical properties of  $(\text{Ba,Sr})\text{TiO}_3$  films prepared by liquid source chemical vapor deposition, *IEICE Trans. Electronics*, E81-C47, (1998) pp. 497.
- Yoon, Y.-K.; Kim, D., Allen, M. G., Kenney, J. S. & Hunt, A.T. (2003). *IEEE Trans. Microwave Theory Tech.*, Vol. 51, (December 2003) pp. 2568-2576.
- York, B. & Pond, J. (2000). IMS Workshop Notes: Ferroelectric Materials and Microwave Applications. 2000 International Microwave Symposium (IMS), Boston, MA, June 11-16, 2000.
- Zeng, J.M.; Lin, C.L., Li, J.H. & Li, K. (1999). Low temperature preparation of barium titanate thin films by a novel sol-gel-hydrothermal method, *Materials Lett.*, Vol. 38, No. 2, (January 1999) pp. 112-115.
- nGimat (2006). A low cost analog phase shifter product family for military, commercial and public safety applications, *Microwave Journal*, Product release article, Vol. 49, No. 3, (March 2006) pp. 152-156.
- Zhao, Z.; Jiang, Y., Wang, X., Choi, K. & Hunt, A.T. (2006). Epitaxial growth of ferroelectric thin films by combustion chemical vapor deposition and their electrical properties, *Proceedings of the 15<sup>th</sup> IEEE Int'l Symp. Applications of Ferroelectrics (ISAF)*, pp. 356-359, Sunset Beach, NC, Jul. 30-Aug. 2, (2006) IEEE, Piscataway, NJ.
- Zhao, Z.; Wang, X., Choi, K. & Hunt, A.T. (2007). Ferroelectric Phase Shifters at 20 and 30 GHz, *IEEE Trans. Microwave Theory Tech*, Vol. 55, No. 2, (2007) pp. 430-437.
- Zheng, G.; Papapolymerou, J.; Tentzeris, M.M. (2003). Wideband coplanar waveguide RF probe pad to microstrip transitions without via holes, *IEEE Micro. Wireless Comp. Lett.*, Vol. 13, No. 12, (December 2003) pp. 544-546.



## **Microwave and Millimeter Wave Technologies from Photonic Bandgap Devices to Antenna and Applications**

Edited by Igor Minin

ISBN 978-953-7619-66-4

Hard cover, 468 pages

**Publisher** InTech

**Published online** 01, March, 2010

**Published in print edition** March, 2010

The book deals with modern developments in microwave and millimeter wave technologies, presenting a wide selection of different topics within this interesting area. From a description of the evolution of technological processes for the design of passive functions in millimetre-wave frequency range, to different applications and different materials evaluation, the book offers an extensive view of the current trends in the field. Hopefully the book will attract more interest in microwave and millimeter wave technologies and simulate new ideas on this fascinating subject.

### **How to reference**

In order to correctly reference this scholarly work, feel free to copy and paste the following:

Stanis Courreges, Zhiyong Zhao, Kwang Choi, Andrew Hunt and John Papapolymerou (2010). Electronically Tunable Ferroelectric Devices for Microwave Applications, *Microwave and Millimeter Wave Technologies from Photonic Bandgap Devices to Antenna and Applications*, Igor Minin (Ed.), ISBN: 978-953-7619-66-4, InTech, Available from: <http://www.intechopen.com/books/microwave-and-millimeter-wave-technologies-from-photonic-bandgap-devices-to-antenna-and-applications/electronically-tunable-ferroelectric-devices-for-microwave-applications>

**INTECH**  
open science | open minds

### **InTech Europe**

University Campus STeP Ri  
Slavka Krautzeka 83/A  
51000 Rijeka, Croatia  
Phone: +385 (51) 770 447  
Fax: +385 (51) 686 166  
[www.intechopen.com](http://www.intechopen.com)

### **InTech China**

Unit 405, Office Block, Hotel Equatorial Shanghai  
No.65, Yan An Road (West), Shanghai, 200040, China  
中国上海市延安西路65号上海国际贵都大饭店办公楼405单元  
Phone: +86-21-62489820  
Fax: +86-21-62489821

© 2010 The Author(s). Licensee IntechOpen. This chapter is distributed under the terms of the [Creative Commons Attribution-NonCommercial-ShareAlike-3.0 License](#), which permits use, distribution and reproduction for non-commercial purposes, provided the original is properly cited and derivative works building on this content are distributed under the same license.